



Research article

High power illumination system for uniform, isotropic and real time controlled irradiance in photoactivated processes research

Carlos Sáenz^{a,b,*}, Begoña Hernández^{a,b}, Diego Sanz-Carrillo^b, Ismael Pellejero^b, Luis M. Gandía^{a,b}

^a Department of Science, Public University of Navarre, Campus Arrosadía, 31006 Pamplona, Spain

^b Institute for Advanced Materials and Mathematics (INAMAT²), Public University of Navarre, Campus Arrosadía, 31006 Pamplona, Spain

ARTICLE INFO

Keywords:

Integrating sphere
Uniform illumination
Isotropic illumination
Actinometry
Photocatalysis

ABSTRACT

In the study of photocatalytic and photoactivated processes and devices a tight control on the illumination conditions is mandatory. The practical challenges in the determination of the necessary photonic quantities pose serious difficulties in the characterization of catalytic performance and reactor designs and configurations, compromising an effective comparison between different experiments.

To overcome these limitations, we have designed and constructed a new illumination system based in the concept of the integrating sphere (IS). The system provides uniform and isotropic illumination on the sample, either in batch or continuous flow modes, being these characteristics independent of the sample geometry. It allows direct, non-contact and real time determination of the photonic quantities as well as versatile control on the irradiance values and its spectral characteristics. It can be also scaled up to admit samples of different sizes without affecting its operational behaviour.

The performance of the IS system has been determined in comparison with a second illumination system, mounted on an optical bench, that provides quasi-parallel beam (QPB) nearly uniform illumination in tightly controlled conditions. System performance is studied using three sample geometries: a standard quartz cuvette, a thin straight tube and a microreactor by means of potassium ferrioxalate actinometry. Results indicate that the illumination geometry and the angular distribution of the incoming light greatly affect the absorption at the sample. The sample light absorption efficiency can be obtained with statistical uncertainties of about 3% and in very good agreement with theoretical estimations.

1. Introduction

At research stage it is necessary to evaluate the performance of photocatalytic and photoactivated systems under well-defined conditions [1] that include a tight control on the illumination of the target sample under study. This is mandatory for characterization purposes, aiming for standardization [2], but also necessary for more efficient scale-up for industrial application [3]. Despite the intense activity in the field, there are presently no standard procedures serving as a working guide and the problem of sample

* Corresponding author.

E-mail address: csaenz@unavarra.es (C. Sáenz).

<https://doi.org/10.1016/j.heliyon.2024.e31309>

Received 27 October 2023; Received in revised form 14 May 2024; Accepted 14 May 2024

Available online 20 May 2024

2405-8440/© 2024 The Author(s). Published by Elsevier Ltd. This is an open access article under the CC BY-NC-ND license (<http://creativecommons.org/licenses/by-nc-nd/4.0/>).

illumination has been necessarily addressed by each research group. Adopted solutions are specifically designed for a given particular problem, resulting in a plethora of illumination systems with varying characteristics [4].

Determination of the efficiency of a particular reaction or reactor design, i.e. the reaction rates obtained for a given illumination, is of the utmost importance. It can be quantified as an overall quantum yield but its evaluation may be difficult, particularly in heterogeneous systems [5]. Other parameters like the photonic efficiency, the ratio of absorbed and incident photon numbers, are in principle easier to determine and of practical interest [6,7]. In principle, photon quantities, e.g. photon fluence rate, can be easily derived from the corresponding radiometric quantities, e.g. irradiance, provided detailed knowledge of the spectral composition of the incoming radiation is available. This information, required to compare experiments performed under different experimental conditions [8,9], is not always easy to determine.

In practice, these data are rarely known with the required accuracy. Descriptions of illuminating systems may lack of the necessary detailed information, referring solely to the lamp model or its basic technical characteristics, which is clearly insufficient to evaluate the irradiance at the illuminated surface, even approximately [10]. Simple calculations involving strong assumptions like irradiance uniformity, normal incidence or the validity of the inverse square law for extended sources, that do not generally hold, will have unacceptable uncertainties [9,11,12,10]. Detailed irradiance calculations based in radiative transfer theory are complex and specific to each particular illumination-reactor geometry. Even simplified models are still complex and exhibit large uncertainties [13].

Calculations cannot replace actual measurements [9], but precise irradiance measurements are not straightforward. Portable UV radiometers with detached sensor probes [14–19] are not wavelength sensitive detectors, typically adjusted for the solar spectral emission and having relatively large uncertainties, up to 5%-10% in good quality systems [20,21]. More importantly, their measuring heads are relatively large, even larger than many samples or devices, and exact positioning at the point of interest is a difficult task, particularly in tightly packed sample-light source geometries.

A single measurement cannot inform about the spatial irradiance distribution across the sample surface. Having a uniform illumination is of great interest since reaction kinetics frequently depends on the irradiance values [22–28] or localized thermal effects [3]. Although irradiance uniformity is recognized as an important characteristic affecting the experimental performance [29,3] its experimental determination is not simple. It is rarely reported [30] and, in general, it is only qualitatively justified or simply assumed [31,32,19].

To complicate matters, obtaining appreciable reaction rates usually require high irradiance levels that, in most cases, are obtained at the expense of uniformity. For instance, uniformity can be improved increasing the distance between the sample and the light source. However, this reduces the irradiance at the sample, forcing prohibitive long irradiation times. Approaching the light source to the reaction vessel increases the irradiation levels, but compromises uniformity. The problem can be alleviated using multiple light sources, like LED strips and arrays [24,33–36]. It has been shown that illumination uniformity depends critically on the size of the sample, the distribution of light sources in the array and on the array-sample distance [24,37,38] and it is very poor if light sources are too close to the sample surface. Samples and light sources can be also covered by aluminium foils or enclosed in cavities having mirror like interior walls [39–42]. These solutions effectively provide higher irradiances but uniformity, in particular in the presence of mirror-like multiple reflections, is very difficult to guarantee and, above all, to measure.

Ultimately, reactions take place inside a container, for example, a cuvette, a parallel plate chamber or a complex shaped channel in a microreactor. Light reaching the surface of the container must propagate through the container's material before reaching the internal, active volume. Refraction and reflection phenomena strongly depend on the angle of incidence of the incoming light and on the refractive indexes, that are very large in the UV region, e.g. $n = 1.56$ for quartz [43]. This fact substantially complicates its modelling and these effects are usually neglected [44]. Although normal light incidence is generally assumed, it is rarely accomplished in real experiments and such approximation may lead to large uncertainties. Finally, a very efficient reaction necessarily implies an efficient light absorption, making light attenuation inside the sample an important factor to be considered [19]. Actual photon rates or photon dose inside the reaction volume are best determined by actinometric methods that can be successfully applied to small-scale microreactors and microfluidic devices [45,9,11]. Difficulties in relating actinometric and radiometric quantities are then inherited from the assumptions taken in the modelling of the illumination system or in the actual measurements of the irradiance levels [46].

Besides a uniform, well determined irradiance at the sample, during the characterization stage it is also desirable to have control on the irradiance values and on the spectral or temporal characteristics of the illumination. In case of fixed power lamps, irradiance values can be simply modified shielding part of the lamp source [47], or intervening neutral filters between the light source and the sample, a method somewhat limited by filter availability [46,48,30]. Systems using LED sources offer a more flexible solution, since irradiance can be controlled by tuning the LED driving current. Spectral control of the illuminating source is also important because of the wavelength dependent response of photoactive and photocatalytic reactions and particularly interesting for efficient light management in applications to work with natural sunlight [12,49]. Using light sources with different technology and characteristics, like Xe lamps, LEDs or Hg lamps [39,50–55] require different experimental arrangements, making comparison and interpretation of the results very difficult. In this sense, broadband light sources combined with spectral filters [56] or LED arrays with different peak emission wavelengths [57,58] are a better solution. Finally, the effect of temporal variations of the irradiance values is of importance in experiments performed under natural sunlight [59] or in the presence of deactivation [18]. Real time control on the illumination could be also of interest in connection to low residence time devices for rapid optimization of reaction parameters [60].

In this work, we propose a different approach to obtain uniform, isotropic, controlled and real-time measurable irradiance on the studied sample. Our solution is based on the technology of integrating spheres, applied to the specific problem of photocatalytic and photoactivated studies. Integrating spheres, or Ulbricht spheres, are designed to provide uniform and homogeneous irradiance in their

interior volume and their theory is well established [61–63]. Their versatility can be exploited in many light-related applications like phosphorescence, photoluminescence or photodegradation experiments [64–69].

2. Methods

An integrating sphere (IS) illumination system has been designed and constructed to provide uniform, isotropic and real time measured irradiance in the studied sample. The system has been studied in comparison with a quasi-parallel beam (QPB) illumination system, where light reaches the sample in a nearly parallel beam and irradiance parameters can be tightly controlled. In both cases, actual photon irradiances have been determined by standard potassium ferrioxalate actinometry and compared with direct spectral irradiance measurements. In order to disentangle illumination and sample effects, three different sample geometries have been studied: batch measurements under total absorption conditions in a standard quartz cuvette and two continuous flow systems: a tube geometry and a microreactor.

2.1. Samples

For batch measurements we have used a High Performance Quartz Glass cuvette (CV) (Hellma 117F, UV/VIS 200-2500 nm) with the standard 10 mm × 10 mm internal cross section and 1.25 mm wall thickness. It is a sealable model with a screw cap, since measurements in the integrating sphere are performed with the cuvette in horizontal position.

The tube (TB) sample is a silicone cylindrical tube with internal and external diameters of 1.0 mm and 2.9 mm, respectively. It is a common geometry in photactivated experiments, where tubes are typically coiled around the light source [70,9,11,52,71].

The microreactor (MR) sample was built in a 40 mm × 40 mm × 5 mm polydimethylsiloxane (PDMS) slab using 3D printing technologies [18]. It consists of a 345.4 mm long, serpentine-shaped channel with circular, 1.38 mm in diameter, cross section and an internal volume of 0.517 cm³.

Black UV absorbing tape was used to cover feeding tubes and connection tips as well as selected portions of the samples to have precise control on the irradiated surface. Light refraction in the sample surface and within the sample is unavoidable. In particular, lensing effects when parallel beams, as in the QPB system, or isotropic light, like in the IS system, reach the sample have been taken into account for a proper interpretation of the results. Samples and details of light propagation in their interfaces are further described in the Supporting Information.

2.2. Light management

To reduce systematic errors when comparing them, both QPB and IS illumination systems mounted the same M365LP1 UV LED sources (Thorlabs Inc.). Their emission peaks at 365 nm with a Full Width at Half Maximum (FWHM), of 9 nm. Their spectral response, output stability and irradiance modelling have been checked in the laboratory (see Supporting Information). QPB and IS systems also mount the same light detector, a miniature spectrometer (Stellar Net BLUE-wave) connected to a UV-VIS-NIR cosine corrector (Stellar Net CR2, 200-1700 nm, 180° FOV) with a UV-VIS fibre-optic cable (190-1100 nm, 600 μm core diameter). Spectral irradiance data are collected in the 270-1100 nm range at $\Delta\lambda = 0.5$ nm intervals. The whole system was factory calibrated (NIST traceable source) for absolute irradiance measurements. Irradiance E (W m⁻²) and photon flux density (photon irradiance) E_p (m⁻² s⁻¹) are computed directly from the spectral irradiance data as described in the Supporting Information.

2.3. Actinometer

Determination of the actual photon flux reaching the sample active volume has been done using actinometry. We have used potassium ferrioxalate, K₃[Fe(C₂O₄)₃]·3H₂O, a well-studied actinometer [72–74] that fits the requirements of both batch and continuous flow experiments [9,11]. Preparation of the 6 mM (C₀) ferrioxalate solution was performed according to the IUPAC recommendations [75]. This concentration guarantees a constant quantum yield, $\Phi = 1.26 \pm 0.03$ at $\lambda = 365$ nm [72,76], for a cuvette with a 1 cm path length [77]. The same solution was used for all experiments and conversion fractions have been also kept sufficiently low (< 12%) so that light absorption in the reaction products of potassium ferrioxalate can be neglected [78]. Further details are given in the Supporting Information.

2.4. Quasi-Parallel Beam (QPB) illumination system

The QPB illumination system, described in detail in the Supporting Information, was mounted on a small optical table with the M365LP1 LED and the samples (CV, TB and MR) aligned and separated a distance $z = 25.0$ cm (Fig. 1a). At this distance, the LED can be considered a point-like light source and radiometric calculations are straightforward. Maximum angle of incidence on the samples is small, ensuring quasi-normal light incidence. In the particularly important case of the CV sample, the maximum angle of incidence is $\theta_{max} = 4.2^\circ$ and light transmittance through its walls can be easily calculated as $T = 0.947$. The entire system was enclosed in a protective lightproof box made of black, UV absorbing material to reduce internal reflections. LED and samples were further separated by an internal wall, made with the same material, with a small window for illumination (Fig. 1c). Exposure times were externally controlled by an electro-mechanical shutter directly screwed to the LED output. To evaluate the average irradiance on the samples, corrections due to the small separation between the detector and the sample centre (Figs. 1b and 1d) and due to the

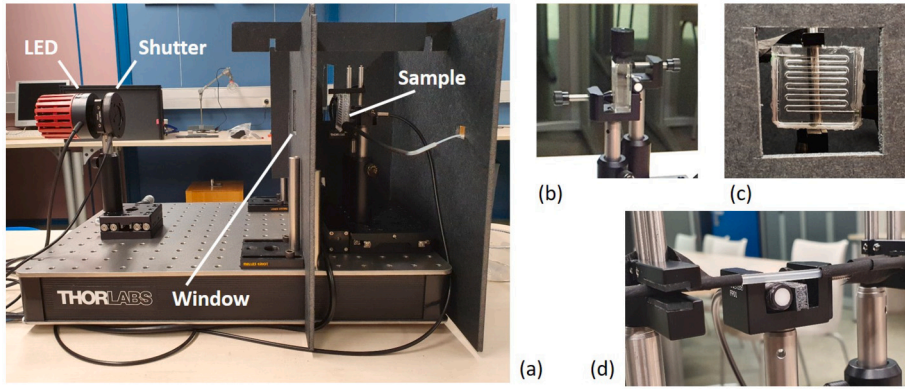


Fig. 1. QPB illumination system, without the protective light absorbing box (a). Samples CB (b) and TB (d) are shown in their sample holders, together with the light detector head. The MR sample (c) has been pictured through the window of the internal wall of the system.

irradiance uniformity over the sample have been taken into account and are, regardless the sample, less than 0.5% (see Supporting Information).

2.5. The Integrating Sphere (IS) illumination system

In essence, an integrating sphere (IS) is a spherical cavity with its interior surface covered by a diffusing, highly reflecting material. Light entering the sphere, or produced inside it, suffers multiple diffuse reflections in the cavity walls, losing all directional information and providing a uniform isotropic luminous energy density within the cavity’s volume and, in consequence, a uniform and isotropic irradiance. Integrating spheres cannot be perfect, closed spheres because openings, called ports, are required to introduce light into the sphere or to locate measurement equipment like a photodetector. Ports are not covered by the internal reflective material and produce a reduction in the effective reflecting area. However, their effect is relatively small as long as the area covered by ports remains small compared to the total area of the sphere.

The relationship between the light power inserted inside an integrating sphere P_0 and the irradiance E_{IS} in the inner surface of the integrating sphere is [79]

$$E_{IS} = \frac{P_0}{\pi A} M, \tag{1}$$

where A is the sphere’s internal surface and M is the sphere’s multiplier factor, given by

$$M = \frac{\rho}{1 - \rho(1 - f)}, \tag{2}$$

with ρ the reflectance of the sphere’s interior surface and f the fraction of A covered by ports.

Port fraction f can be reduced by increasing the sphere’s internal area A , but according to equation (1) this reduces the irradiance inside the sphere. As an acceptable compromise, the area covered by ports should not exceed 5% of the sphere’s area, i.e. $f \leq 0.05$. For a given port fraction f the multiplier factor M is a strictly increasing function of the sphere’s internal reflectance ρ . Larger irradiances are obtained if high, close to one, reflectance materials are used as sphere coatings. Depending on the wavelength range, high reflectance diffusing materials with $\rho \geq 0.95$ are available.

The spherical geometry together with a lambertian diffusing coating creates a uniform radiation field everywhere inside the sphere [80,81]. A sample placed in its centre is expected to receive a uniform irradiance E_s . On the other hand, a light detector D properly located in the sphere’s inner surface will provide a direct measurement of the irradiance value at the IS inner surface, i.e. $E_D = E_{IS}$. It can be shown (Supporting Information) that irradiance at the sample can be obtained from the irradiance at the detector as

$$E_s = \rho E_D \tag{3}$$

Since irradiance is uniform inside the sphere, $E_{avg} = E_s$ with very good approximation. According to equation (3), for a perfectly reflecting diffusing coating ($\rho = 1$) we simply have $E_{avg} = E_s = E_D$. In real situations ρ is very close but slightly less than 1. Ultimately, this small difference is unimportant since the measured irradiance is calibrated with the actinometric measurements.

2.5.1. Design and construction

The integrating sphere, with an internal diameter of 150 mm, has been constructed in micro carbon reinforced nylon (Markforged Onyx) using a 3D printer (Fig. 2). It consists of two separated hemispheres. The lower hemisphere (LH) has two light input ports, a light detector port and two thin, stainless steel, horizontal parallel wires that serve as simple sample holder. The LH is fixed to a heavy stainless steel plaque, providing a sturdy, stable base during measurements. Two upper hemispheres (UH1 and UH2) have been constructed. One of them (UH2) has two extra light input ports, placed at right angles respect to the light input ports of LH, to

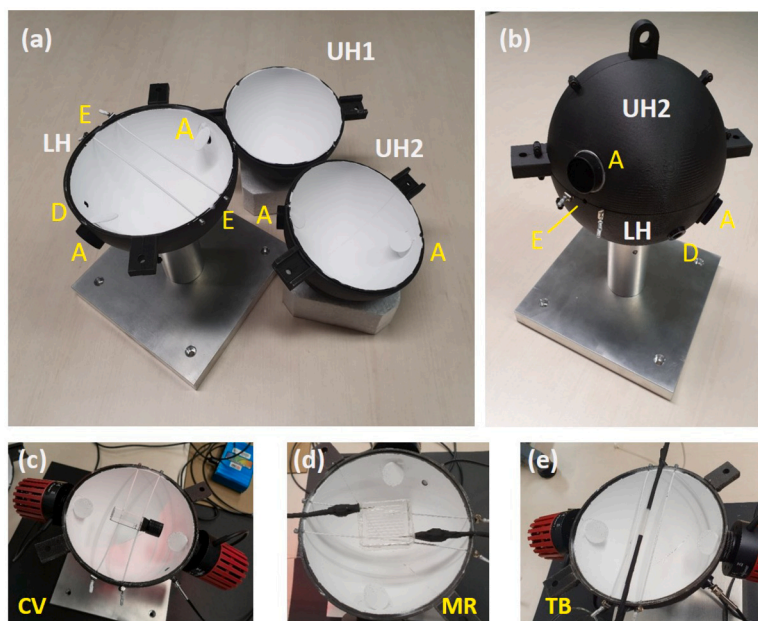


Fig. 2. (a) IS hemispheres showing the lower, fixed hemisphere (LH) and the two upper hemispheres, one without holes (UH1) and another prepared to hold two extra light sources (UH2). (b) Closed IS with hemispheres LH and UH2. Labels indicate light ports (A), spectrophotometer port (D) and input holes for feeding tubes (E). (c-e) Samples are positioned at the centre of the IS.

accept extra light sources if necessary. The other upper hemisphere (UH1) is devoid of ports or holes. All actinometric measurements were performed with UH1. Small circular baffles redirect the input light to the internal surface of the IS, avoiding direct, non diffuse illumination of the sample or the light detector. The internal surface of each hemisphere, including thread adapters, baffles, detector-mounting ring and sample holder wires, was spray painted with barium sulphate BaSO_4 . Up to 15 layers were deposited to ensure a very good diffusing, reflecting coating. Further construction details can be found in the Supporting Information.

2.5.2. Basic operational characteristics

The IS system offers a tight control on the spectral characteristics of the illumination, limited only by the type and number of the light sources that can be connected to the input ports. As an example, Fig. 3 shows the spectral irradiance measured in the IS with different light sources, including combinations of LEDs with different wavelengths or a single Xe lamp source connected to the IS with a filter holder having different spectral filters.

In addition, high multiplier factors allow high irradiances at relatively small light powers. Irradiances up to 180 W m^{-2} , several times the total UV solar irradiance at the Earth's surface, have been measured in this IS system using a single M365LP1 LED source. This shows that the IS system is much more efficient than the QPB system. Since there are four light source ports available in the sphere, much higher values can be obtained. However 180 W m^{-2} is the maximum irradiance we can presently measure with our equipment.

2.5.3. Irradiance uniformity inside the sphere

The characteristics of the irradiance inside the IS have been tested with several basic tests (see Supporting Information). Measurements at random locations inside the integrating sphere show that irradiance uniformity, determined as the standard deviation [38,36], is better than 1.8%. This can be compared with a reported uniformity of 6.4%, also calculated as the standard deviation across the sample, for an optimized uniformity/total irradiance using a rectangular array of 192 LEDs [38]. Irradiance is also nearly independent on the exact location of the sample. Moving a CV sample along the sample holder produces small variations (standard deviation) in the measured irradiance of 0.50% (empty cuvette) to 1.1% (cuvette filled with actinometer). This means that the IS behaviour is highly insensitive to the sample position and accurate positioning of the sample is unnecessary.

3. Results and discussion

In order to facilitate the analysis it is desirable to have a comparable range of actinometer conversion fraction in the experiments. For this purpose, and due to the intrinsic differences between QPB and IS illumination systems and between samples, energy/photon dose was controlled, according to the Bunsen-Roscoe law of reciprocity, varying either the irradiance or the exposure time. A summary of the operational parameters for each illumination system and sample is shown in Table 1.

Figs. 4, 5 and 6 show that the actinometer conversion fraction X is linearly related to the fluence $H = Et$, and photon fluence $H_p = E_p t$, for the CV, TB and MR samples under both QPB and IS illumination. The fitting parameters corresponding to $X = aH_p + b$

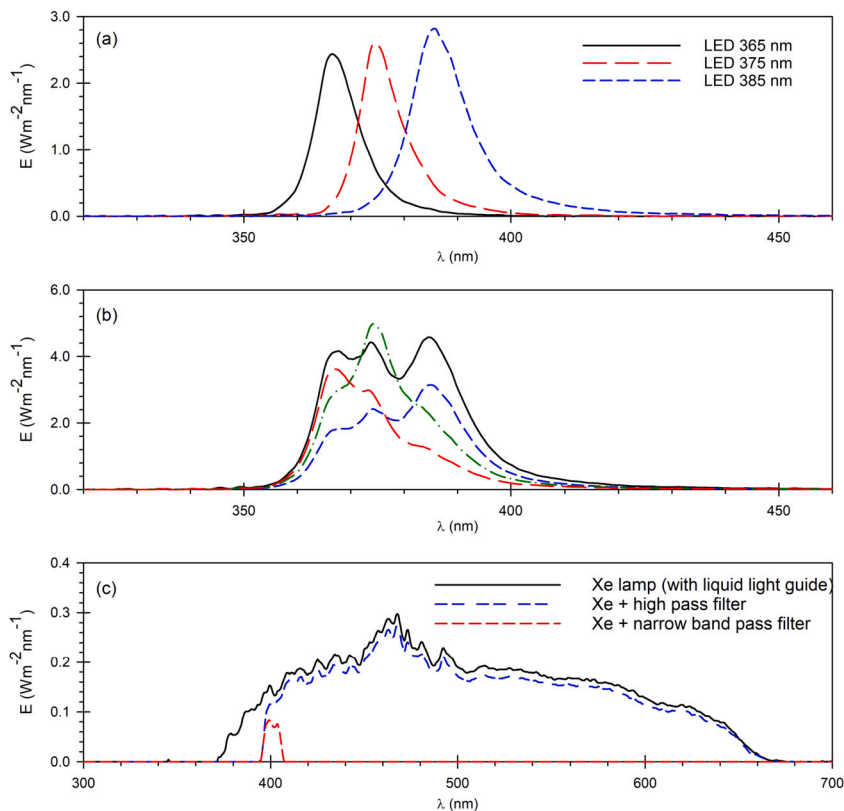


Fig. 3. Spectral irradiance inside the IS equipped with different light sources. (a) Individual spectra of three narrow band LEDs centred at 365, 375 and 385 nm. (b) Four different (simultaneous) combinations of the same three LEDs varying their relative intensities. (c) Spectral irradiance with a Xenon lamp directly inserted in the IS using a liquid light guide and in combination with a high pass filter (visible light only) or a narrow band pass filter (centred at 400 nm).

Table 1

Experimental conditions for CV, TB and MR samples during experiments in QPB and IS illumination geometries.

Parameter	QPB			IS		
	CV	TB	MR	CV	TB	MR
t (s)	10-340	8.5	62	50	1.5	62
Q (mL/h)	-	10	30	-	60	30
E (Wm^{-2})	5.1-5.3	2.6-6.2	0.21-0.57	0.53-9.0	2.1-16.7	0.16-0.89
E_p ($\times 10^{18} \text{ m}^{-2} \text{ s}^{-1}$)	9.5-9.8	4.9-11.5	0.38-1.1	0.99-16.7	3.9-31.1	0.30-1.7
X (%)	0.3-8.8	1.7-3.7	0.6-1.8	0.7-10.8	0.8-6.6	1.7-11.0
V (cm^3)	4.50	0.024	0.517	4.50	0.024	0.517
S (cm^2)	3.375	0.300	4.767	13.50	0.9425	14.974
S/V (m^{-1})	75.0	1250	922	300	3927	2896

are listed in the two upper sections of Table 2. Similarly, Table 3 shows the fitting results in case of $X = aH + b$. Coefficients of determination R^2 are always greater than 0.99, confirming the linear behaviour. Furthermore, within statistical uncertainties, the constant term b is always compatible with 0. This is what we expect, since X is already corrected with the blank sample and corresponds to the conversion fraction due to irradiation only. In consequence, actinometer conversion fraction X is simply proportional to the photon fluence H_p or fluence H .

The proportionality constant, the slope a in the linear fits, varies with sample. This is a consequence of their different geometries, sizes and materials, a point that will be discussed later in more detail. For a given sample, there are also differences in a between QPB and IS illumination geometries, since it is not the same to illuminate a sample from just one side with a nearly parallel light beam than irradiating the sample from every direction with an isotropic light source. In the CV sample for instance, only one side, with area S_{QPB} , is illuminated in QPB conditions. Inside the IS four sides, with area $S_{IS} = 4S_{QPB}$ are illuminated. If, for a given fluence, conversion in QPB and IS should depend solely on the illuminated surface we would expect a ratio $a_{IS}/a_{QPB} = S_{IS}/S_{QPB} = 4$. However, as shown in Table 2, the actual value is $a_{IS}/a_{QPB} = 4.88 \pm 0.09$. The same result is obtained using the fluence (Table 3). If we define the ratio

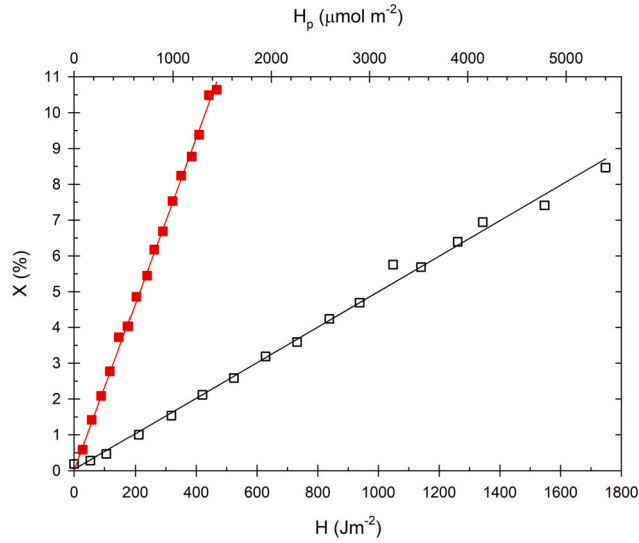


Fig. 4. Actinometer conversion fraction X as a function of photon fluence H_p and fluence H for the CV sample in QPB (hollow black squares) and IS (solid red squares) systems. Linear fits shown as solid lines.

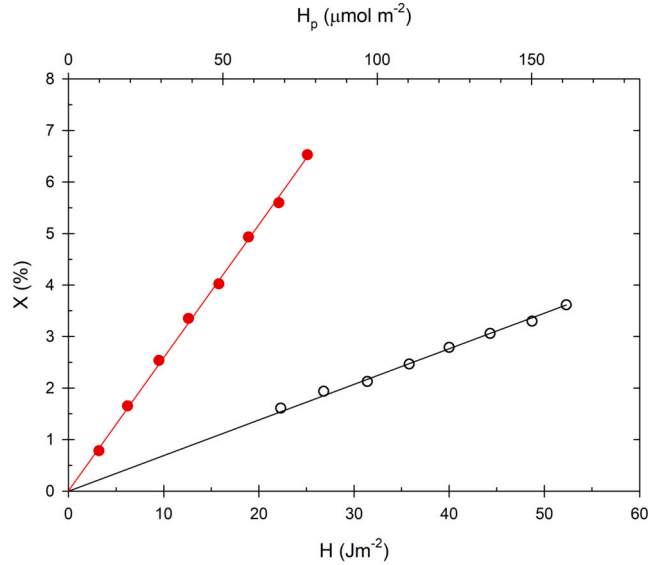


Fig. 5. Actinometer conversion fraction X as a function of photon fluence H_p and fluence H for the TB sample in QPB (hollow black circles) and IS (solid red circles) systems. Linear fits shown as solid lines.

$$\eta = \frac{a_{IS}/a_{QPB}}{S_{IS}/S_{QPB}}, \quad (4)$$

the value $\eta_{CV} = 1.22 \pm 0.02$ is obtained for the CV sample, which is greater than 1 beyond statistical uncertainties. The same situation is found in case of the TB and MR samples. Because of the circular cross section of the actinometer volume, the geometric ratio of the irradiated surfaces is $S_{IS}/S_{QPB} = \pi$. However, in both cases the ratio a_{IS}/a_{QPB} is greater, as shown in Table 2, being $\eta_{TB} = 1.20 \pm 0.03$ (TB) and $\eta_{MR} = 1.22 \pm 0.04$ (MR). Identical results are obtained using the fitting results with fluence H (Table 3) because for such a narrow band light source H and H_p are nearly proportional.

Interestingly, the ratios η for the three samples are equal within statistical uncertainties. Since the three samples are so different in size, shape and material, it is reasonable to assume that the value of η is, very approximately, sample independent and that it depends principally on the illumination system. With this assumption, and taking into account that the three experimental values are statistically indistinguishable, we can safely take their average $\eta = 1.21 \pm 0.05$ as a reference value. This factor is simply a calibration factor that relates the irradiance measured by the detector at the IS walls with the actual irradiance obtained from the actinometry. It includes the effective reflectance of the IS walls and the lensing effects due to the isotropic illumination (see Supporting Information)

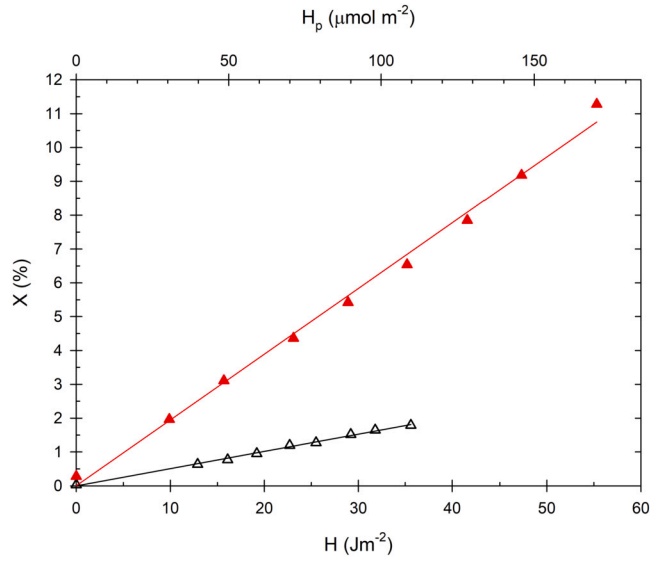


Fig. 6. Actinometer conversion fraction X as a function of photon fluence H_p and fluence H for the MR sample in QPB (hollow black triangles) and IS (solid red triangles) systems. Linear fits shown as solid lines.

Table 2

Results of the linear fit $X = aH_p + b$ with X the actinometer conversion fraction and H_p the photon fluence for the QPB and IS experiments. Uncertainties quoted as standard errors.

Parameter	CV	TB	MR
QPB Illumination			
a_{QPB} ($\mu\text{mol}^{-1} \text{m}^2$)	0.00161 ± 0.00003	0.0223 ± 0.0004	0.0165 ± 0.0004
b_{QPB}	0.04 ± 0.07	0.00 ± 0.05	0.00 ± 0.03
R^2	0.9957	0.9975	0.9961
IS Illumination			
a_{IS} ($\mu\text{mol}^{-1} \text{m}^2$)	0.0078 ± 0.0001	0.084 ± 0.001	0.063 ± 0.002
b_{IS}	0.01 ± 0.06	0.00 ± 0.04	0.0 ± 0.2
R^2	0.9984	0.9991	0.9945
Ratios			
a_{IS}/a_{QPB}	4.88 ± 0.09	3.76 ± 0.08	3.8 ± 0.1
S_{IS}/S_{QPB}	4.0	π	π
$\eta = (a_{IS}/a_{QPB})/(S_{IS}/S_{QPB})$	1.22 ± 0.02	1.20 ± 0.03	1.22 ± 0.04

Table 3

Results of the linear fit $X = aH + b$ with X the actinometer conversion fraction and H the fluence for the QPB and IS experiments. Uncertainties quoted as standard errors.

Parameter	CV	TB	MR
QPB Illumination			
a_{QPB} ($\text{J}^{-1} \text{m}^2$)	0.00496 ± 0.00008	0.069 ± 0.001	0.051 ± 0.001
b_{QPB}	0.04 ± 0.07	0.00 ± 0.05	0.00 ± 0.03
R^2	0.9957	0.9977	0.9960
IS Illumination			
a_{IS} ($\text{J}^{-1} \text{m}^2$)	0.0242 ± 0.0002	0.259 ± 0.003	0.194 ± 0.006
b_{IS}	0.01 ± 0.06	0.00 ± 0.04	0.0 ± 0.2
R^2	0.9984	0.9991	0.9944
Ratios			
a_{IS}/a_{QPB}	4.87 ± 0.09	3.7 ± 0.1	3.8 ± 0.1
S_{IS}/S_{QPB}	4.0	π	π
$\eta = (a_{IS}/a_{QPB})/(S_{IS}/S_{QPB})$	1.22 ± 0.02	1.19 ± 0.03	1.22 ± 0.05

Table 4Linear fit results of $X = \epsilon(\eta X_{ps}) + b$ with $\eta_{QPB} = 1$ and $\eta_{IS} = 1.21$.

Sample		ϵ	b	R^2
Cuvette	QPB	0.97 ± 0.02	0.04 ± 0.07	0.9957
	IS	1.00 ± 0.01	0.01 ± 0.06	0.9984
Tube	QPB	0.83 ± 0.02	0.00 ± 0.05	0.9975
	IS	0.84 ± 0.01	0.00 ± 0.05	0.9991
Microreactor	QPB	0.85 ± 0.02	0.00 ± 0.03	0.9961
	IS	0.87 ± 0.03	0.0 ± 0.2	0.9947

Illumination and sample effects can be further investigated comparing the measured actinometer conversion fraction X with the theoretical estimations X_{th} . In total absorption conditions, X_{th} is usually computed as [9]

$$X_{th} = \frac{S}{V} \frac{\Phi}{C_0} E_p t T f, \quad (5)$$

where S is the area of the irradiated surface and V is the actinometer volume. Both quantities are defined by the geometry of the sample and enter the equation as the surface to volume ratio S/V that is typically known with uncertainties of the order of 1%. Similar accuracy can be assumed for the actinometer quantum yield Φ and concentration C_0 . The product of the photon irradiance at the sample surface E_p and the irradiation time t is the photon fluence H_p . The sample transmittance T takes into account that not all photons reaching the surface reach the active, interior volume. Finally, the factor f measures the absorption efficiency in the active volume. Its value is $f = 1$ in total absorption conditions, like in the CV sample, but in general $f < 1$, like in the TB and MR samples. In those cases, estimating f using the Beer-Lambert law and an effective path-length l_{eff} is possible, but prone to uncertainties if calculations of l_{eff} do not properly take into account refraction and reflection phenomena inside the sample. Notice that some effects, like lens effects in the TB sample, even for QPB illumination, are not clearly included in any of these factors.

It may be useful to define an ideal or perfect sample (ps) devoid of all sample effects that are difficult to evaluate. In connection with equation (5) it should be a sample that, regardless its geometry, has perfect transmittance ($T = 1$) and total absorption ($f = 1$). For this hypothetical sample, every photon reaching its surface is absorbed and the actinometer conversion fraction X_{ps} would be simply

$$X_{ps} = \frac{S}{V} \frac{\Phi}{C_0} E_p t \quad (6)$$

Clearly, the perfect sample does not represent a real sample, but if photon irradiance is well defined X_{ps} can be accurately determined. In order to obtain the conversion fraction for a real sample, and comparing with equation (5), we should multiply X_{ps} by the product Tf . Instead, we introduce a factor ϵ that incorporates the effect of transmittance, lack of total absorption, lensing or any other sample related phenomena affecting the light absorption efficiency. Furthermore, we also introduce the factor η , defined in equation (4), and associated to the illumination system or illumination geometry. With these factors, the actinometer conversion fraction is given by

$$X = \eta \epsilon X_{ps} \quad (7)$$

Here ϵ is an overall measure of the sample effectiveness in collecting light. For complex sample designs, theoretical estimations of ϵ clearly present the same problems as the theoretical estimations of T or f . In the present experiment, calculations are simple only in the case of the CV sample under QPB illumination. In this case, because of the nearly normal incidence in both external and internal surfaces, the light collecting area S can be considered to be equal to the geometric area S_{QPB} . Total absorption is guaranteed in the CV sample so that $f = 1$. Finally, since light incidence is nearly normal in both the external and internal surfaces, the sample transmittance is $T = 0.947$ (Supporting Information). Therefore, in case of the CV sample, we expect equation (5) to be valid with $\epsilon = \epsilon_{CV} = 0.947$. In addition, in normal incidence and in absence of refraction, we can also assume $\eta_{QPB} = 1$ and take simply $\eta_{IS} = 1.21 \pm 0.05$.

According to equation (7), if we plot the actinometer conversion fraction X versus the factor ηX_{ps} , with X_{ps} given by equation (6) and $\eta = \eta_{QPB} = 1$ or $\eta = \eta_{IS} = 1.21 \pm 0.05$ depending on the illumination system, we expect a linear relationship with slope equal to ϵ . These plots, for the CV, TB and MR samples are shown in Fig. 7 and the corresponding linear fits in Table 4. In all cases, the constant term b vanishes within uncertainties and $R^2 > 0.99$, meaning that X and ηX_{ps} are effectively proportional, with ϵ the proportionality factor.

For each sample, the factor η effectively brings data to a common line and the values of ϵ are almost equal within statistical errors, regardless of the illumination system. In case of the CV sample and QPB conditions, $\epsilon_{QPB} = 0.97 \pm 0.02$ is in good agreement with the expected theoretical value $\epsilon = T = 0.947$ if only the sample transmittance in normal incidence is taken into account. The slightly higher $\epsilon_{IS} = 1.00 \pm 0.01$ is statistically equivalent to ϵ_{QPB} within errors. For the TB and MR samples, despite their different and more complex structure, an even better agreement is obtained and $\epsilon_{QPB} = \epsilon_{IS}$ in both cases. Therefore, it can be concluded that the influence of the illumination geometry and the sample properties can be factorized, within present uncertainties, as $\eta \epsilon$. The factor η encompasses the effects of the geometric distribution of the incoming light. The factor ϵ contains the sample related effects with respect to its optical behaviour. We must be aware that this factorization, seemingly valid within the present accuracy

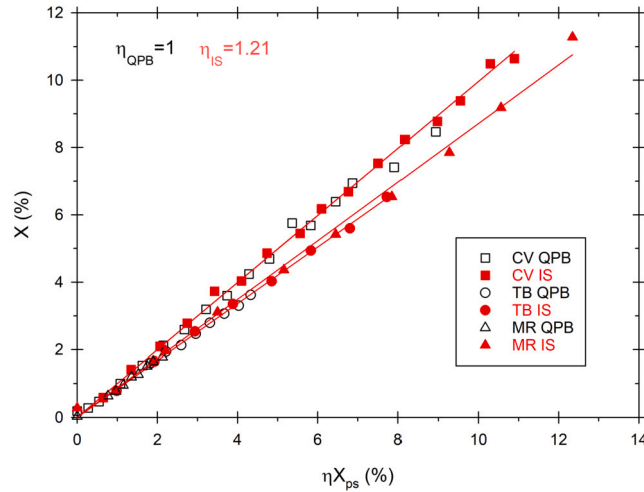


Fig. 7. Actinometer conversion fraction X as a function of ηX_{ps} with $\eta_{QPB} = 1$ and $\eta_{IS} = 1.21$. Linear fits of IS data are shown in red.

($\approx 2\%$) can not be strictly true since there is an intrinsic connection between illumination geometry and refraction phenomena in the sample surface. However, this connection ultimately depends on the refractive index which, for the same wavelengths, is similar in all samples.

It is remarkable that the sample dependent factor ϵ is equal, within errors, for the TB and MR samples. Naive calculations in tubular geometries, assuming normal incidence and neglecting refraction or total reflection, provide effective path lengths inside the active volume that are proportional to the tube diameter. Since the diameter of the microreactor channel is 1.38 times the tube inner diameter we should expect a more efficient photon absorption in the microreactor and a ratio $\epsilon_{MR}/\epsilon_{TB} \approx 1.38$, in contradiction with the experimental value $\epsilon_{MR}/\epsilon_{TB} \approx 1$. Actually, lensing effects on its curved surface compensate the smaller diameter of the TB sample. On the other hand, the almost exact numerical coincidence of their respective ϵ values must be regarded as accidental. In any case, this clearly shows that refraction, and the consequent lensing phenomena, must be properly taken into account to avoid large biases in the theoretical estimations.

The agreement of theoretical and experimental values of the sample factor ϵ for the CV sample suggests that it can be used as a valid reference for any other sample. Taking values relative to the CV sample makes them insensitive to common factors, like the concentration and quantum efficiency of the actinometer, and their associated uncertainties. In addition, it makes unnecessary to use the less efficient QPB system for sample characterization.

In particular, for an illuminating system, like the IS system, the ratio of the actinometer conversion fraction X of a given sample with respect to the conversion fraction X_{CV} in the CV sample does not depend on the illumination factor η , that cancels out

$$\frac{X_{Sample}}{X_{CV}} = \frac{\epsilon_{Sample}}{\epsilon_{CV}} \frac{X_{ps,Sample}}{X_{ps,CV}} \quad (8)$$

For the same actinometer and for a given photon fluence H_p , the ratio $X_{ps,Sample}/X_{ps,CV}$ is simply the ratio of their respective surface to volume ratios, that can be accurately determined. If we now define the sample effect relative to the CV sample, ϵ_r as

$$\epsilon_r = \frac{\epsilon_{Sample}}{\epsilon_{CV}} \quad (9)$$

Then

$$\frac{X_{Sample}}{X_{CV}} = \epsilon_r \frac{(S/V)_{Sample}}{(S/V)_{CV}} \quad (10)$$

Table 5 shows the relative sample factors ϵ_r for each illumination geometry. For the CV data we have obviously $\epsilon_r = 1$, and results are only shown to emphasize the corresponding uncertainties. Since ϵ_{CV} was already very close to 1 for QPB and IS systems, the relative values ϵ_r for the TB and MR samples are very similar to the absolute ϵ values in Table 4. Using the CV sample as a reference, only the more efficient IS illumination system is required to completely characterize the efficiency associated to a particular sample.

4. Conclusions

We have designed and constructed an illuminating system based on the concept of the integrating sphere (IS) for the study of photoactivated and photocatalytic reactions and reactor designs, in either batch or continuous flow regime. The IS system provides uniform and isotropic illumination on the sample surface with little dependence on the sample geometry and size. It provides efficient illumination in the 4π sr solid angle, increasing the efficiency, but can be equally used with single sided reactors or reactors with other acceptance angles.

Table 5

Sample efficiency relative to the CV efficiency, ϵ_r , obtained in the QPB and IS illumination systems.

Sample	ϵ_r	
	QPB	IS
CV	1.00 ± 0.02	1.00 ± 0.01
TB	0.83 ± 0.02	0.82 ± 0.01
MR	0.83 ± 0.03	0.84 ± 0.03

It has been calibrated with standard actinometry and validated against a quasi parallel beam (QPB) illumination system, where calculations and measurements in total absorption conditions and nearly normal incidence can be accurately related. Actinometric determination of absorbed photon fluxes in three different sample geometries irradiated in the IS and QPB system exhibits good agreement and internal consistency. It has been shown that the effect of the illumination geometry and of the sample characteristics in the overall reaction efficiency can be disentangled. This is particularly useful in reactor design where, once calibrated, only the much more efficient IS illumination system is needed.

Light sources are themselves external to the system, offering a flexible platform to control the spectral characteristics of the incident light over a wide spectral range and admitting a variety of light sources, maybe in combination, using several light input ports. Furthermore, irradiance is monitored in real time and spectral basis and very high irradiance values can be easily achieved. These characteristics do not affect the illumination geometry at the sample surface and nearly eliminate problems associated with lamp cooling systems.

Refraction phenomena at the sample, which is particularly important in the UV due to the high refractive indexes at these wavelengths, have a strong dependence on the angular distribution of the incoming light. Since refraction is unavoidable, detailed comparison between experiments requires a precise knowledge of the illumination geometry. In this regard the IS system provides not only uniform, but also isotropic illumination, devoid of preferred directions, making it ideal for characterization purposes.

CRedit authorship contribution statement

Carlos Sáenz: Writing – original draft, Investigation, Formal analysis, Data curation, Conceptualization. **Begoña Hernández:** Writing – review & editing, Investigation, Formal analysis, Data curation, Conceptualization. **Diego Sanz-Carrillo:** Methodology, Investigation, Formal analysis, Data curation. **Ismael Pellejero:** Methodology, Funding acquisition, Conceptualization. **Luis M. Gandía:** Writing – review & editing, Funding acquisition.

Declaration of competing interest

The authors declare the following financial interests/personal relationships which may be considered as potential competing interests: Co-author Luis M. Gandía is a Section Editor for Heliyon. If there are other authors, they declare that they have no known competing financial interests or personal relationships that could have appeared to influence the work reported in this paper.

Data availability statement

All relevant data is included in the manuscript and/or in the supplementary material.

Acknowledgement

Authors thank the financial support from the Spanish Agencia Estatal de Investigación and Spanish Ministerio de Ciencia e Innovación, MCIN/AEI/ 10.13039/501100011033/ and FEDER “Una manera de hacer Europa”, grants PID2019-106687RJ-I00 and PID2021-127265OB-C21, and Gobierno de Navarra, grant PC091-092 FOREST2+. L.M.G. thanks Banco de Santander and UPNA for their financial support under “Programa de Intensificación de la Investigación 2018” initiative.

Appendix A. Supplementary material

Supplementary material related to this article can be found online at <https://doi.org/10.1016/j.heliyon.2024.e31309>.

References

- [1] S.K. Loeb, P.J. Alvarez, J.A. Brame, E.L. Cates, W. Choi, J. Crittenden, D.D. Dionysiou, Q. Li, G. Li-Puma, X. Quan, D.L. Sedlak, T. David Waite, P. Westerhoff, J.H. Kim, The technology horizon for photocatalytic water treatment: sunrise or sunset?, *Environ. Sci. Technol.* 53 (6) (2019) 2937–2947, https://doi.org/10.1021/ACS.EST.8B05041/ASSET/IMAGES/LARGE/ES-2018-05041U_0004.JPEG.
- [2] M.L. Bechev, N. Costarramone, T. Pigot, S. Lacombe, Gas-phase photooxidation: reactors and materials, *Chem. Eng. Technol.* 39 (2016) 26–38, <https://doi.org/10.1002/CEAT.201500349>.

- [3] R. Binjhade, R. Mondal, S. Mondal, Continuous photocatalytic reactor: critical review on the design and performance, *J. Environ. Chem. Eng.* 10 (3) (2022) 107746, <https://doi.org/10.1016/J.JECE.2022.107746>.
- [4] L. Buglioni, F. Raymenants, A. Slattery, S.D. Zondag, T. Noël, Technological innovations in photochemistry for organic synthesis: flow chemistry, high-throughput experimentation, scale-up, and photoelectrochemistry, *Chem. Rev.* 122 (2022) 2752–2906, <https://doi.org/10.1021/ACS.CHEMREV.1C00332>.
- [5] N. Serpone, R. Terzian, D. Lawless, P. Kenneppohl, G. Sauvé, On the usage of turnover numbers and quantum yields in heterogeneous photocatalysis, *J. Photochem. Photobiol. A, Chem.* 73 (1) (1993) 11–16, [https://doi.org/10.1016/1010-6030\(93\)80027-7](https://doi.org/10.1016/1010-6030(93)80027-7).
- [6] N. Serpone, G. Sauvé, R. Koch, H. Tahiri, P. Pichat, P. Piccinini, E. Pelizzetti, H. Hidaka, Standardization protocol of process efficiencies and activation parameters in heterogeneous photocatalysis: relative photonic efficiencies ζ_r , *J. Photochem. Photobiol. A, Chem.* 94 (2–3) (1996) 191–203, [https://doi.org/10.1016/1010-6030\(95\)04223-7](https://doi.org/10.1016/1010-6030(95)04223-7).
- [7] A. Mills, S. Le Hunte, An overview of semiconductor photocatalysis, *J. Photochem. Photobiol. A, Chem.* 108 (1) (1997) 1–35, [https://doi.org/10.1016/S1010-6030\(97\)00118-4](https://doi.org/10.1016/S1010-6030(97)00118-4).
- [8] T. Aillet, K. Loubiere, O. Dechy-Cabaret, L. Prat, Photochemical synthesis of a “cage” compound in a microreactor: rigorous comparison with a batch photoreactor, *Chem. Eng. Process. Process Intensif.* 64 (2013) 38–47, <https://doi.org/10.1016/j.cep.2012.10.017>.
- [9] T. Aillet, K. Loubiere, O. Dechy-Cabaret, L. Prat, Accurate measurement of the photon flux received inside two continuous flow microphotoreactors by actinometry, *Int. J. Chem. React. Eng.* 12 (1) (2014), <https://doi.org/10.1515/IJCRE-2013-0121>.
- [10] J. Fernández-Catalá, G. Garrigós-Pastor, A. Berenguer-Murcia, D. Cazorla-Amorós, Photo-microfluidic chip reactors for propene complete oxidation with TiO₂ photocatalyst using UV-LED light, *J. Environ. Chem. Eng.* 7 (5) (2019) 103408, <https://doi.org/10.1016/J.JECE.2019.103408>.
- [11] B. Wriedt, D. Kowalczyk, D. Ziegenbalg, Experimental determination of photon fluxes in multilayer capillary photoreactors, *ChemPhotoChem* 2 (10) (2018) 913–921, <https://doi.org/10.1002/CPTC.201800106>.
- [12] C.J. Bueno-Alejo, J.L. Hueso, R. Mallada, I. Julian, J. Santamaria, High-radiance LED-driven fluidized bed photoreactor for the complete oxidation of n-hexane in air, *Chem. Eng. J.* 358 (2019) 1363–1370, <https://doi.org/10.1016/J.CEJ.2018.09.223>.
- [13] H.A. Irazoqui, M.A. Isla, A.E. Cassano, Simplified extense source model for photoreactor analysis and design, *Ind. Eng. Chem. Res.* 39 (11) (2000) 4260–4271, <https://doi.org/10.1021/ie9907876>.
- [14] R. Gorges, S. Meyer, G. Kreisel, Photocatalysis in microreactors, *J. Photochem. Photobiol. A, Chem.* 167 (2004) 95–99, <https://doi.org/10.1016/J.JPHOTOCHEM.2004.04.004>.
- [15] C.C. Lo, C.H. Hung, C.S. Yuan, Y.L. Hung, Parameter effects and reaction pathways of photoreduction of co₂ over tio₂/so₄²⁻ photocatalyst, *Chin. J. Catal.* 28 (2007) 528–534, [https://doi.org/10.1016/S1872-2067\(07\)60046-1](https://doi.org/10.1016/S1872-2067(07)60046-1).
- [16] M. Krivec, A. Pohar, B. Likozar, G. Dražić, Hydrodynamics, mass transfer, and photocatalytic phenol selective oxidation reaction kinetics in a fixed TiO₂ microreactor, *AIChE J.* 61 (2) (2015) 572–581, <https://doi.org/10.1002/AIC.14648>.
- [17] R. Chen, L. Li, X. Zhu, H. Wang, Q. Liao, M.X. Zhang, Highly-durable optofluidic microreactor for photocatalytic water splitting, *Energy* 83 (2015) 797–804, <https://doi.org/10.1016/J.ENERGY.2015.02.097>.
- [18] A. Castedo, E. Mendoza, I. Angurell, J. Llorca, Silicone microreactors for the photocatalytic generation of hydrogen, *Catal. Today* 273 (2016) 106–111, <https://doi.org/10.1016/J.CATTOD.2016.02.053>.
- [19] X. Zhan, C. Yan, Y. Zhang, G. Rinke, G. Rabsch, M. Klumpp, A.I. Schäfer, R. Dittmeyer, Investigation of the reaction kinetics of photocatalytic pollutant degradation under defined conditions with inkjet-printed TiO₂ films – from batch to a novel continuous-flow microreactor, *React. Chem. Eng.* 5 (9) (2020) 1658–1670, <https://doi.org/10.1039/D0RE00238K>.
- [20] M. Sengupta, A. Habte, C. Gueymard, S. Wilbert, D. Renne, *Best practices handbook for the collection and use of solar resource data for solar energy applications: Second edition*, Tech. rep., National Renewable Energy Lab, 2017.
- [21] F. Tang, X. Yang, A “deactivation” kinetic model for predicting the performance of photocatalytic degradation of indoor toluene, o-xylene, and benzene, *Build. Environ.* 56 (2012) 329–334, <https://doi.org/10.1016/J.BUILDENV.2012.04.001>.
- [22] D.F. Ollis, E. Pelizzetti, N. Serpone, Photocatalyzed destruction of water contaminants, *Environ. Sci. Technol.* 25 (9) (1991) 1522–1529, https://doi.org/10.1021/ES00021A001/ASSET/ES00021A001.FP.PNG_V03.
- [23] I.K. Konstantinou, T.A. Albanis, TiO₂-assisted photocatalytic degradation of azo dyes in aqueous solution: kinetic and mechanistic investigations: a review, *Appl. Catal. B, Environ.* 49 (1) (2004) 1–14, <https://doi.org/10.1016/J.APCATB.2003.11.010>.
- [24] Z. Wang, J. Liu, Y. Dai, W. Dong, S. Zhang, J. Chen, CFD modeling of a UV-LED photocatalytic odor abatement process in a continuous reactor, *J. Hazard. Mater.* 215–216 (2012) 25–31, <https://doi.org/10.1016/J.JHAZMAT.2012.02.021>.
- [25] N. Tsuchiya, K. Kuwabara, A. Hidaka, K. Oda, K. Katayama, Reaction kinetics of dye decomposition processes monitored inside a photocatalytic microreactor, *Phys. Chem. Chem. Phys.* 14 (14) (2012) 4734–4741, <https://doi.org/10.1039/C2CP23979E>.
- [26] A. Visan, D. Raffiean, W. Ogieglo, R.G. Lammertink, Modeling intrinsic kinetics in immobilized photocatalytic microreactors, *Appl. Catal. B, Environ.* 150–151 (2014) 93–100, <https://doi.org/10.1016/J.APCATB.2013.12.003>.
- [27] A. Castedo, I. Uriz, L. Soler, L.M. Gandía, J. Llorca, Kinetic analysis and CFD simulations of the photocatalytic production of hydrogen in silicone microreactors from water-ethanol mixtures, *Appl. Catal. B, Environ.* 203 (2017) 210–217, <https://doi.org/10.1016/J.APCATB.2016.10.022>.
- [28] A.L. Liu, Z.Q. Li, Z.Q. Wu, X.H. Xia, Study on the photocatalytic reaction kinetics in a TiO₂ nanoparticles coated microreactor integrated microfluidics device, *Talanta* 182 (2018) 544–548, <https://doi.org/10.1016/J.TALANTA.2018.02.028>.
- [29] B.M. da Costa Filho, V.J. Vilar, Strategies for the intensification of photocatalytic oxidation processes towards air streams decontamination: a review, *Chem. Eng. J.* 391 (2020) 123531, <https://doi.org/10.1016/J.CEJ.2019.123531>.
- [30] M.L. Satuf, J. Macagno, A. Manassero, G. Bernal, P.A. Kler, C.L. Berli, Simple method for the assessment of intrinsic kinetic constants in photocatalytic microreactors, *Appl. Catal. B, Environ.* 241 (2019) 8–17, <https://doi.org/10.1016/J.APCATB.2018.09.015>.
- [31] H. Fu, C. Pan, W. Yao, Y. Zhu, Visible-light-induced degradation of rhodamine B by nanosized Bi₂WO₆, *J. Phys. Chem. B* 109 (47) (2005) 22432–22439, <https://doi.org/10.1021/JP052995J>.
- [32] C. Passalía, O.M. Alfano, R.J. Brandi, Integral design methodology of photocatalytic reactors for air pollution remediation, in: *Molecules* 2017, in: Vol. 22, 2017, p. 945.
- [33] M. Hajaghazadeh, V. Vaiano, D. Sannino, H. Kakooei, R. Sotudeh-Gharebagh, P. Ciambelli, Heterogeneous photocatalytic oxidation of methyl ethyl ketone under UV-A light in an LED-fluidized bed reactor, *Catal. Today* 230 (2014) 79–84, <https://doi.org/10.1016/J.CATTOD.2013.08.020>.
- [34] M. Martín-Sómer, C. Pablos, R. van Grieken, J. Marugán, Influence of light distribution on the performance of photocatalytic reactors: led vs Mercury lamps, *Appl. Catal. B, Environ.* 215 (2017) 1–7, <https://doi.org/10.1016/J.APCATB.2017.05.048>.
- [35] B. Ramos, J.G.M. Carneiro, L.I. Nagamati, A.C.S. Teixeira, Development of intensified flat-plate packed-bed solar reactors for heterogeneous photocatalysis, *Environ. Sci. Pollut. Res. Int.* 28 (2021) 24023–24033, <https://doi.org/10.1007/S11356-020-11806-9/FIGURES/8>.
- [36] T. Matiazzo, K. Ramaswamy, V.J. Vilar, N. Padoin, C. Soares, Radiation field modeling of the NETmix milli-photocatalytic reactor: effect of LEDs position over the reactor window, *Chem. Eng. J.* 429 (2022), <https://doi.org/10.1016/J.CEJ.2021.131670>.
- [37] A. Roibu, R.B. Morthala, M.E. Leblebici, D. Koziej, T.V. Gerven, S. Kuhn, Design and characterization of visible-light led sources for microstructured photoreactors, *React. Chem. Eng.* 3 (2018) 849–865, <https://doi.org/10.1039/C8RE00165K>.
- [38] T. Claes, A. Dilissen, M.E. Leblebici, T. Van Gerven, Translucent packed bed structures for high throughput photocatalytic reactors, *Chem. Eng. J.* 361 (2019) 725–735, <https://doi.org/10.1016/J.CEJ.2018.12.107>.

- [39] M.A. Lillo-Ródenas, N. Bouazza, A. Berenguer-Murcia, J.J. Linares-Salinas, P. Soto, A. Linares-Solano, Photocatalytic oxidation of propene at low concentration, *Appl. Catal. B, Environ.* 71 (3–4) (2007) 298–309, <https://doi.org/10.1016/J.APCATB.2006.10.004>.
- [40] J.Y. Do, Y. Im, B.S. Kwak, J.Y. Kim, M. Kang, Dramatic CO₂ photoreduction with H₂O vapors for CH₄ production using the TiO₂ (bottom)/Fe-TiO₂ (top) double-layered films, *Chem. Eng. J.* 275 (2015) 288–297, <https://doi.org/10.1016/J.CEJ.2015.03.066>.
- [41] C.C. Le, M.K. Wismer, Z.C. Shi, R. Zhang, D.V. Conway, G. Li, P. Vachal, I.W. Davies, D.W. MacMillan, A general small-scale reactor to enable standardization and acceleration of photocatalytic reactions, *ACS Cent. Sci.* 3 (2017) 647–653, <https://doi.org/10.1021/ACSCENTSCI.7B00159>.
- [42] M. González-Esguevillas, D.F. Fernández, J.A. Rincón, M. Barberis, O.D. Frutos, C. Mateos, S. García-Cerrada, J. Agejas, D.W. Macmillan, Rapid optimization of photoredox reactions for continuous-flow systems using microscale batch technology, *ACS Cent. Sci.* 7 (2021) 1126–1134, <https://doi.org/10.1021/ACSCENTSCI.1C00303>.
- [43] G. Ghosh, Dispersion-equation coefficients for the refractive index and birefringence of calcite and quartz crystals, *Opt. Commun.* 163 (1–3) (1999) 95–102, [https://doi.org/10.1016/S0030-4018\(99\)00091-7](https://doi.org/10.1016/S0030-4018(99)00091-7).
- [44] A.E. Cassano, C.A. Martín, R.J. Brandi, O.M. Alfano, Photoreactor analysis and design: fundamentals and applications, *Ind. Eng. Chem. Res.* 34 (1995) 2155–2201, <https://doi.org/10.1021/IE00046A001>.
- [45] Y.Z. Yang, C.H. Chang, H. Idriss, Photo-catalytic production of hydrogen from ethanol over M/TiO₂ catalysts (M = Pd, Pt or Rh), *Appl. Catal. B, Environ.* 67 (3–4) (2006) 217–222, <https://doi.org/10.1016/J.APCATB.2006.05.007>.
- [46] A. Manassero, M.L. Satuf, O.M. Alfano, Kinetic modeling of the photocatalytic degradation of clofibrate in a slurry reactor, *Environ. Sci. Pollut. Res. Int.* 22 (2) (2015) 926–937, <https://doi.org/10.1007/S11356-014-2682-5/FIGURES/9>.
- [47] L. Jia, Y. Jin, J. Li, Z. Wei, M. Chen, J. Ma, Study on high-efficiency photocatalytic degradation of oxytetracycline based on a spiral microchannel reactor, *Ind. Eng. Chem. Res.* 61 (2022) 554–565, <https://doi.org/10.1021/ACS.IECR.1C03495>.
- [48] A. Manassero, S.M. Zacañas, M.L. Satuf, O.M. Alfano, Intrinsic kinetics of clofibrate photocatalytic degradation in a fixed-film reactor, *Chem. Eng. J.* 283 (2016) 1384–1391, <https://doi.org/10.1016/J.CEJ.2015.08.060>.
- [49] Q. Wang, C. Pornrungrroj, S. Linley, E. Reisner, Strategies to improve light utilization in solar fuel synthesis, *Nat. Energy* 7 (1) (2022) 13–24, <https://doi.org/10.1038/S41560-021-00919-1>.
- [50] C.C. Lo, C.H. Hung, C.S. Yuan, J.F. Wu, Photoreduction of carbon dioxide with H₂ and H₂O over TiO₂ and ZnO in a circulated photocatalytic reactor, *Sol. Energy Mater. Sol. Cells* 91 (2007) 1765–1774, <https://doi.org/10.1016/J.SOLMAT.2007.06.003>.
- [51] Y. Su, V. Hessel, T. Noël, A compact photomicroreactor design for kinetic studies of gas-liquid photocatalytic transformations, *AIChE J.* 61 (2015) 2215–2227, <https://doi.org/10.1002/AIC.14813>.
- [52] Y. Chen, O. de Frutos, C. Mateos, J.A. Rincon, D. Cantillo, C.O. Kappe, Continuous flow photochemical benzylic bromination of a key intermediate in the synthesis of a 2-oxazolidinone, *ChemPhotoChem* 2 (2018) 906–912, <https://doi.org/10.1002/CPTC.201800114>.
- [53] J. Fernández-Catalá, Ángel Berenguer-Murcia, D. Cazorla-Amorós, Photocatalytic oxidation of VOCs in gas phase using capillary microreactors with commercial TiO₂ (P25) fillings, *Materials* 11 (2018), <https://doi.org/10.3390/MA11071149>.
- [54] B.M. da Costa Filho, A.L. Araujo, S.P. Padrão, R.A. Boaventura, M.M. Dias, J.C.B. Lopes, V.J. Vilar, Effect of catalyst coated surface, illumination mechanism and light source in heterogeneous TiO₂ photocatalysis using a mini-photoreactor for n-decane oxidation at gas phase, *Chem. Eng. J.* 366 (2019) 560–568, <https://doi.org/10.1016/J.CEJ.2019.02.122>.
- [55] O. Sacco, V. Vaiano, L. Rizzo, D. Sannino, Intensification of ceftriaxone degradation under UV and solar light irradiation in presence of phosphorus based structured catalyst, *Chem. Eng. Process. Process Intensif.* 137 (2019) 12–21, <https://doi.org/10.1016/J.CEP.2019.01.011>.
- [56] J. Albero, E. Domínguez, A. Corma, H. García, Continuous flow photoassisted CO₂ methanation, *Sustain. Energy Fuels* 1 (6) (2017) 1303–1307, <https://doi.org/10.1039/C7SE00246G>.
- [57] C.P. Haas, T. Roeder, R.W. Hoffmann, U. Tallarek, Light as a reaction parameter – systematic wavelength screening in photochemical synthesis, *React. Chem. Eng.* 4 (2019) 1912–1916, <https://doi.org/10.1039/C9RE00339H>.
- [58] R. Radjagobalou, V.D.D.S. Freitas, J.F. Blanco, F. Gros, J. Dauchet, J.F. Cornet, K. Loubiere, A revised 1d equivalent model for the determination of incident photon flux density in a continuous-flow led-driven spiral-shaped microreactor using the actinometry method with Reinecke's salt, *J. Flow Chem.* 11 (2021) 357–367, <https://doi.org/10.1007/S41981-021-00179-W/FIGURES/10>.
- [59] T.V. Nguyen, J.C. Wu, C.H. Chiou, Photoreduction of CO₂ over Ruthenium dye-sensitized TiO₂-based catalysts under concentrated natural sunlight, *Catal. Commun.* 9 (10) (2008) 2073–2076, <https://doi.org/10.1016/J.CATCOM.2008.04.004>.
- [60] C.W. Coley, M. Abolhasani, H. Lin, K.F. Jensen, Material-efficient microfluidic platform for exploratory studies of visible-light photoredox catalysis, *Angew. Chem., Int. Ed. Engl.* 56 (2017) 9847–9850, <https://doi.org/10.1002/ANIE.201705148>.
- [61] R. Ulbricht, Die Bestimmung der mittleren räumlichen Lichtintensität durch nur eine Messung, 1900.
- [62] D.K. Edwards, R.D. Roddick, K.E. Nelson, J.T. Gier, Integrating sphere for imperfectly diffuse samples, *J. Opt. Soc. Am.* 51 (11) (1961) 1279–1288, <https://doi.org/10.1364/JOSA.51.001279>.
- [63] D.G. Goebel, Generalized integrating-sphere theory, *Appl. Opt.* 6 (1967) 125, <https://doi.org/10.1364/ao.6.000125>.
- [64] N.C. Greenham, I.D. Samuel, G.R. Hayes, R.T. Phillips, Y.A. Kessener, S.C. Moratti, A.B. Holmes, R.H. Friend, Measurement of absolute photoluminescence quantum efficiencies in conjugated polymers, *Chem. Phys. Lett.* 241 (1995) 89–96, [https://doi.org/10.1016/0009-2614\(95\)00584-Q](https://doi.org/10.1016/0009-2614(95)00584-Q).
- [65] J.W. Martin, J.W. Chin, W.E. Byrd, E. Embree, K.M. Kraft, An integrating sphere-based ultraviolet exposure chamber design for the photodegradation of polymeric materials, *Polym. Degrad. Stab.* 63 (1999) 297–304, [https://doi.org/10.1016/S0141-3910\(98\)00109-8](https://doi.org/10.1016/S0141-3910(98)00109-8).
- [66] A.R. Johnson, S.J. Lee, J. Klein, J. Kanicki, Absolute photoluminescence quantum efficiency measurement of light-emitting thin films, *Rev. Sci. Instrum.* 78 (2007), <https://doi.org/10.1063/1.2778614>.
- [67] S. Leyre, E. Coutino-Gonzalez, J.J. Joos, J. Ryckaert, Y. Meuret, D. Poelman, P.F. Smet, G. Durinck, J. Hofkens, G. Deconinck, P. Hanselaer, Absolute determination of photoluminescence quantum efficiency using an integrating sphere setup, *Rev. Sci. Instrum.* 85 (2014), <https://doi.org/10.1063/1.4903852>.
- [68] N. Hasebe, K. Suzuki, H. Horiuchi, H. Suzuki, T. Yoshihara, T. Okutsu, S. Tobita, Absolute phosphorescence quantum yields of singlet molecular oxygen in solution determined using an integrating sphere instrument, *Anal. Chem.* 87 (2015) 2360–2366, <https://doi.org/10.1021/ac5042268>.
- [69] C. Würth, U. Resch-Genger, Determination of photoluminescence quantum yields of scattering media with an integrating sphere: direct and indirect illumination, *Appl. Spectrosc.* 69 (2015) 749–759, <https://doi.org/10.1366/14-07679>.
- [70] F. Lévesque, P.H. Seeberger, Highly efficient continuous flow reactions using singlet oxygen as a “green” reagent, *Org. Lett.* 13 (2011) 5008–5011, https://doi.org/10.1021/OL2017643/SUPPL_FILE/OL2017643_SI_001.PDF.
- [71] X. Pu, B. Zhang, Y. Su, Heterogeneous photocatalysis in microreactors for efficient reduction of nitrobenzene to aniline: mechanisms and energy efficiency, *Chem. Eng. Technol.* 42 (2019) 2146–2153, <https://doi.org/10.1002/CEAT.201800735>.
- [72] C. Hatchard, C. Parker, A new sensitive chemical actinometer - II. potassium ferrioxalate as a standard chemical actinometer, *Proc. R. Soc. Lond. Ser. A, Math. Phys. Sci.* 235 (1956) 518–536, <https://doi.org/10.1098/RSPA.1956.0102>.
- [73] S. Goldstein, J. Rabani, The ferrioxalate and iodide-iodate actinometers in the UV region, *J. Photochem. Photobiol. A, Chem.* 193 (2008) 50–55, <https://doi.org/10.1016/J.JPHOTOCHEM.2007.06.006>.
- [74] J.R. Bolton, M.I. Stefan, P.S. Shaw, K.R. Lykke, Determination of the quantum yields of the potassium ferrioxalate and potassium iodide-iodate actinometers and a method for the calibration of radiometer detectors, *J. Photochem. Photobiol. A, Chem.* 222 (2011) 166–169, <https://doi.org/10.1016/J.JPHOTOCHEM.2011.05.017>.

- [75] H.J. Kuhn, S.E. Braslavsky, R. Schmidt, Chemical actinometry (IUPAC technical report), *Pure Appl. Chem.* 76 (12) (2004) 2105–2146, <https://doi.org/10.1351/PAC200476122105>.
- [76] J. Lee, H.H. Seliger, Quantum yield of the ferrioxalate actinometer, *J. Chem. Phys.* 40 (2004) 519, <https://doi.org/10.1063/1.1725147>.
- [77] C. Weller, S. Horn, H. Herrmann, Effects of Fe(III)-concentration, speciation, excitation-wavelength and light intensity on the quantum yield of iron(III)-oxalato complex photolysis, *J. Photochem. Photobiol. A, Chem.* 255 (2013) 41–49, <https://doi.org/10.1016/j.jphotochem.2013.01.014>.
- [78] B. Wriedt, D. Ziegenbalg, Common pitfalls in chemical actinometry, *J. Flow Chem.* 10 (1) (2020) 295–306, <https://doi.org/10.1007/s41981-019-00072-7>.
- [79] M. Born, E. Wolf, *Principles of Optics: Electromagnetic Theory of Propagation, Interference and Diffraction of Light*, 7th edition, Cambridge University Press, 1999.
- [80] Y.S. Yoo, K.L. Jeong, S. Park, J. Hwang, D.J. Shin, Small integrating sphere light source with high radiance uniformity, *Int. J. Thermophys.* 44 (2023) 1–18, <https://doi.org/10.1007/S10765-023-03227-W/FIGURES/9>.
- [81] J. Chen, G. Sun, S. Liu, G. Zhang, S. Chen, J. Zhang, Q. Liu, Design of integrating sphere uniform light system for solar simulator, *IEEE Photonics J.* 15 (2023), <https://doi.org/10.1109/JPHOT.2023.3237931>.